

Impacts of Inflow Loadings from Heavy Rainfall on Cyanobacteria Overgrowth in Nitrogen-Limited Reservoirs through Field Observation and Numerical Simulation

Tran Thi Lan HUONG^{1,5}, Toshinori TABATA^{2*}, Masayoshi HARADA², Akinori OZAKI³ and Bui Quoc LAP⁴

¹ Department of Agro-environmental Sciences, Graduate School of Bioresource and Bioenvironmental Sciences, Kyushu University, Fukuoka, Japan

² Department of Agro-environmental Sciences, Faculty of Agriculture, Kyushu University, Fukuoka, Japan

³ Institute of Tropical Agriculture, Kyushu University, Fukuoka, Japan

⁴ Faculty of Chemistry and Environment, Thuyloi University, Hanoi, Vietnam

⁵ Faculty of Environment, Thai Nguyen University of Agriculture and Forestry, Thai Nguyen, Vietnam

Abstract

This study presents significant insights into the impact of nitrogen and phosphorus inflow loadings from agricultural activities on phytoplankton proliferation in a hypertrophic reservoir. Over two years, the study meticulously examined seasonal variations in phytoplankton, the dominance of algae species, and nitrogen and phosphorus levels in a reservoir prone to cyanobacterial blooms. The findings revealed that the reservoir was hypertrophic under nitrogen limitation, with temporal nitrogen loadings being the primary cause of algal abnormalities. Cyanobacteria, particularly sensitive to temporary nitrate-nitrogen increases triggered by heavy rainfall, dominated during the study period. A robust ecosystem model, validated through observational data, showed good reproducibility of results. It successfully anticipated shifts in phytoplankton growth patterns, successfully replicating the abnormal proliferation of several algae species. By conducting different nutrient loading scenarios, the research highlighted the crucial role of nitrogen reduction in curbing phytoplankton growth, especially in nitrogen-limited reservoirs. In environments facing severe nitrogen limitation, a simplified ecosystem model proved valuable, aiding in predicting seasonal phytoplankton changes. This study underscores the necessity of accurately identifying limiting factors and implementing targeted strategies to effectively mitigate algal blooms in eutrophic water bodies.

Discipline: Agricultural Engineering

Additional key words: ecosystem model, hypertrophic reservoir, nutrients, phytoplankton, scenario analysis

Introduction

One of the aquatic environmental issues in closed freshwater bodies, such as lakes and reservoirs, is the abnormal proliferation of phytoplankton associated with eutrophication (García-Nieto et al. 2019). Freshwater bodies receive sensitive inflow loadings of nutrients via agricultural runoff, sewage, and industrial discharges, resulting in the overgrowth of algae being highly

responsive to dissolved inorganic phosphorus (DIP) and dissolved inorganic nitrogen (DIN). Especially, cyanobacteria form abnormal algal blooms which concentrate and float on the water surface like green color scum (Aparicio Medrano et al. 2016, Ostrovsky et al. 2020). Consequently, the algal overgrowth causes environmental problems such as landscape damage, obstructions to agricultural water use, and generation of fetid water (Jahan et al. 2009). Additionally, anoxia in an

*Corresponding author: ttabata@bpes.kyushu-u.ac.jp

Received 6 December 2023; accepted 14 May 2024.

aphotic zone occurs because of low transparency derived from the abnormal proliferation of phytoplankton in the heating season, resulting in the acceleration of eutrophication due to the elution of phosphate-phosphorus ($\text{PO}_4\text{-P}$) and ammonium-nitrogen ($\text{NH}_4\text{-N}$) from the anaerobic bottom sediment. It is crucial to propose specific measures for restoring eutrophic water bodies based on understanding the actual circumstances of eutrophic problems.

According to a trophic status classification based on the OECD standard (Organization for Economic Cooperation and Development 1982), many closed freshwater bodies are eutrophic or even hypertrophic (Bhagowati & Ahamad 2019). Lakes and reservoirs tend to receive over-nutrient overloads from dissolved inorganic nitrogen (DIN) rather than dissolved inorganic phosphorus (DIP) (Guildford & Hecky 2000, Havens & Walker 2002). As such, limnology studies concerning water environmental conservation have primarily focused on eutrophic and hypertrophic water bodies in a phosphorus-limited state (Correll 1999). However, some lakes and reservoirs in rural areas tend to be in a nitrogen-limited status because of an increase in inflow loading of DIP derived from excessive fertilizer application of phosphate on farmlands, resulting in prolonged cyanobacteria bloom (Downing & McCauley 1992, Kotani 1992, Sharpley et al. 2006). In addition, due to climate change, the inflow loadings of nutrients derived from agricultural activities would frequently increase in response to localized heavy rainfall, resulting in over-nutrient water areas (Hassanzadeh et al. 2019).

Consequently, many lakes and reservoirs shift towards a hypereutrophic state, representing the highest trophic level. In this state, the water bodies exhibit dense concentrations of algae and macrophytes, rendering them unsuitable for agricultural use and recreational activities. Therefore, urgent countermeasures to hypertrophication would be required to address inhibiting methods for algal bloom by reducing excessive DIN and DIP inflow loading. There are primarily two distinct approaches to effectively achieve this goal. One is to understand the actual circumstances of the hypertrophic water environment to elucidate the generation mechanisms of algal bloom based on detailed field observations. The other is to numerically approach the effects of environmental countermeasures on aquatic ecosystems using a water quality prediction model.

This study focused on an agricultural reservoir with a nitrogen-limited hypertrophic status, where long-term cyanobacteria bloom forms on the extensive water surface in the autumn season of September to November. First, field observations were conducted to understand

the actual circumstances of the hypertrophic water environment from the viewpoint of the seasonal change characteristics of Chl-a relating to inflow loadings of DIN and DIP stemming from rainfall events. Following this, the influences of nutrient inflow loading on the water environment were numerically estimated using the one-box type ecosystem model, recognized as one of the most typical and fundamental water quality prediction models. When simulating seasonal changes in Chl-a based on the ecosystem model, it is necessary to uniquely determine the parameters related to photosynthesis for seasonal changes, such that the dominant species would alter significantly at algal class-differentiated levels corresponding to water temperature and solar radiation. In this study, several temperature zones were set, and the optimal values of the model parameters for phytoplankton growth were determined for each zone. In particular, the difficulty of model application to the hypertrophic reservoir was solved by deciding the dependencies on the water temperature, underwater light intensity of photosynthesis, and maximum algal growth rate, characterized by a dominant species corresponding to the water temperature zone. This proposed ecosystem model was applied to scenario analyses to assess how much the reduction of inflow and initial loadings of DIN and DIP influence the inhibition of phytoplankton overgrowth. The outcomes from these scenario analyses play a vital role in establishing a specific numerical target for the aquatic environment restoration of hypertrophic reservoirs.

Methodology

1. Study site

The targeted closed water body is the No. 7 regulating reservoir (Fig. 1) constructed in 2017 in the Ito Campus of Kyushu University, Japan. This reservoir, where the bottom is flat without a slope and water depths are primarily uniform, has a maximum water depth of approximately 4.5 m, a water surface area of ca. 2,700 m², and a capacity of ca. 12,200 m³ under a water-filled state, and it is used as a water resource for upland irrigation. Because the benefited farmland is located upstream, a storage pump is installed at the bottom bed in the reservoir to supply the irrigation water. The reservoir has two spillways and one inflow entrance for extrinsic water. In the former, the reservoir's water flows out by overflowing broad-crested weirs with a width of 0.45 m, as shown in Figure 1C. The latter means that agricultural drainage from the farmland upstream flows into this reservoir through a box culvert used as a closed conduit drain channel. The reservoir, subject to a robust influx of nutrients, particularly due to the extensive fertilization of

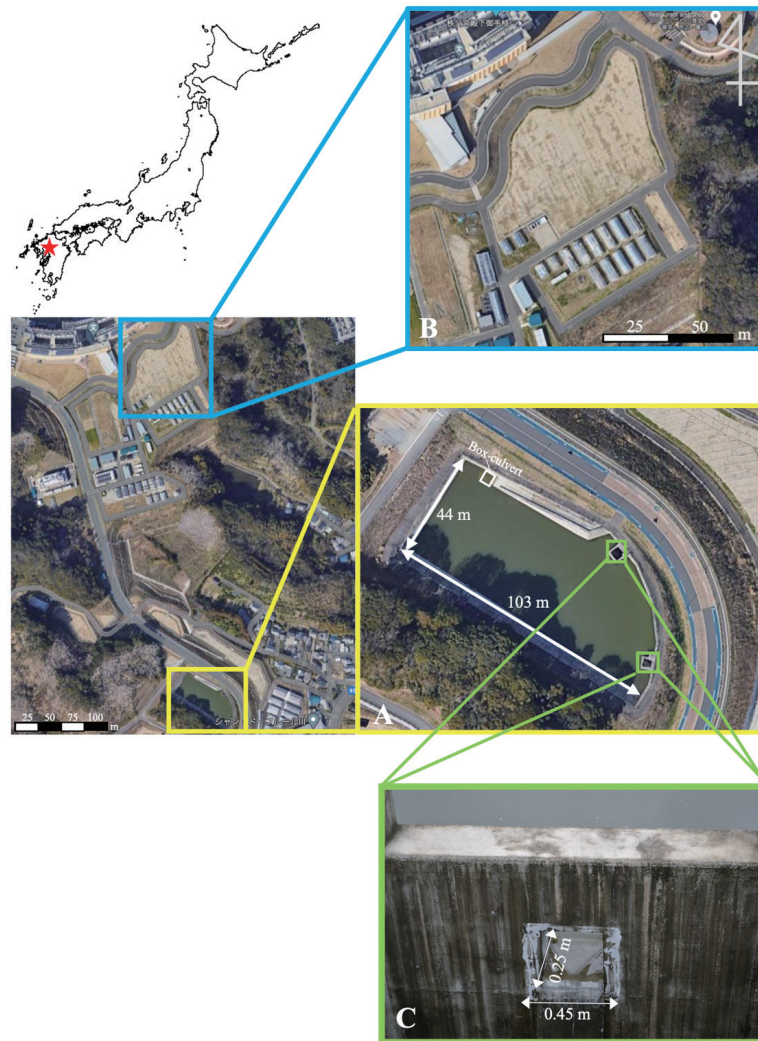


Fig. 1. The location of (A) the target reservoir, (B) upper farmland, and (C) two spillways at the Ito campus, Kyushu University, Japan

the farmland upstream, receives a substantial nutrient load through the box culvert during rainfall.

Since the reservoir's initial impoundment in 2017, high Chl-a concentration, indicative of algal bloom, has been identified by observing the color at the water surface. Additionally, numerous phytoplankton in this reservoir adversely impacted water utilization for upland irrigation, as documented in the following manner. The reservoir's water, including high Chl-a concentration, is pumped up and temporarily stored in an underground embedded farm pond to supply the upstream irrigation water. Many organisms affected by algal death in the light-shielding farm pond caused extreme oxygen consumption, generating hydrogen sulfide under anaerobic conditions with a strong reductive state. A high sulfide concentration (over $150 \mu\text{g/L}$) has been detected with high frequency in the benefited farmland. In the

reservoir, the organic pollution confirmed grey sludge deposition over a wide area at the bottom. Irrigation water with high sulfide concentrations can harm plants by interfering with nutrient uptake, causing damage to the root system, and reacting with metal ions to form toxic metal sulfides (Lamers et al. 2013, Zhang et al. 2017). Therefore, it is urgent to suppress the proliferation of phytoplankton in agricultural reservoirs from the viewpoint of harmful influence on irrigation water use.

2. Field observation

In this study, the periodic observations of water quality parameters related to the eutrophication index were conducted twice a week from April to November in 2019 and 2021 to assess in detail the spatiotemporal changes in the aquatic environment. On-site measurements and water sampling were carried out at the following four

observation points: the water surfaces at the north side, south side, and center, and the bottom at the center of the reservoir. As on-site observations, basic information was obtained using a multi-parameter water quality system (Model 6920, YSI Nanotech), and the transparency was measured using a Secchi disk at the center. The collected water samples were used for the laboratory analysis of two types of Chl-a, $\text{NO}_3\text{-N}$, $\text{NH}_4\text{-N}$, $\text{PO}_4\text{-P}$, total nitrogen (TN), total phosphorus (TP), total organic carbon (TOC), and dissolved organic carbon (DOC). As an indicator representing the total amount of phytoplankton without distinguishing algal classes, Chl-a concentration was measured by the solvent extraction method using *N,N*-dimethylformamide with a fluorophotometer (Aquaflour, Turner Designs). In addition, to roughly understand the phytoplankton composition, in-vivo Chl-a concentrations were analyzed at four class-differentiated algae levels, which consisted of Chlorophyceae, cyanobacteria, diatom/dinoflagellates, and cryptophytes, using a multi-wavelength excitation fluorometer (FluoroProbe, bb-Moldaenke). TOC and DOC were measured using a TOC analyzer (Sievers 900, GE Analytical Instruments) based on a wet ultraviolet oxidation reaction and selective membrane conductometric technology. The water quality parameters excluding Chl-a, TOC, and DOC were measured based on the testing methods for industrial wastewater (JIS K 0102) using an ion chromatograph (Dionex Integrion HPIC, Thermo Fisher Scientific K.K.) and an ultraviolet-visible light spectrophotometer (DR5000, HACH).

In addition to periodic observations, continuous observations with 10-minute intervals were carried out to acquire data concerning water temperature, water depth, and inflow discharge to simulate the water environment using the ecosystem model. The water temperature approximately 1.5 m below the water surface was observed at the center as an overall average reservoir value. A pressure sensor with memory fixed on the bottom logged the water depth at the center. The inflow discharge into the reservoir was continuously measured using a weir-type flowmeter installed inside the box culvert. Furthermore, the following irregular field surveys were conducted to examine the inflow loadings of DIN and DIP from the farmland upstream. Nitrate-nitrogen ($\text{NO}_3\text{-N}$), $\text{NH}_4\text{-N}$, and $\text{PO}_4\text{-P}$ in influent concentrations were measured seven times in 2019 and nine times in 2021 on heavy rainfall events. These results were provided for acquiring the LQ equations describing the relation between inflow loading ($L_X = C_X \cdot Q$) and inflow discharge of water (Q), where the subscript X indicates the water quality parameters of $\text{NO}_3\text{-N}$, $\text{NH}_4\text{-N}$, and $\text{PO}_4\text{-P}$, and C is a concentration of parameter X . Moreover,

basic data (air temperature, solar radiation, and rainfall) was measured at 10-minute intervals on a meteorological observation station near the reservoir's farmland.

3. Water quality prediction model based on a one-box type ecosystem model

Because this study aimed to quantitatively estimate the overgrowth of phytoplankton relating to DIN and DIP inflow loadings stemming from rainfall events, we focused on the process of increasing Chl-a from the summer or autumn season as a targeted calculation period. In most of this period, the vertical profiles of water temperature were almost uniform, and water for the whole area in the water depth direction was in the aerobic state without anoxic water at the bottom. Vertical mixing of water mass in this targeted reservoir completely progressed without forming a stable thermal stratification in the autumn when Chl-a increased to a hypertrophic level due to the overgrowth of cyanobacteria bloom. The reservoir's shallow depth, approximately 4.5 meters, facilitated easy water mixing from bottom to top, increasing oxygen levels. Consequently, a simple box model was chosen for this study. Therefore, it was possible to simulate water quality dynamics without using a three-dimensional or vertical one-dimensional model. The water quality prediction model in this study was a completely mixed-box model based on the ecosystem model (Bui & Dang 2020) and included six state variables: phytoplankton (PP), zooplankton (ZP), particulate nonliving organic matter (POM), dissolved organic matter (DOM), DIP (= $\text{PO}_4\text{-P}$), and DIN (= $\text{NH}_4\text{-N} + \text{NO}_2\text{-N} + \text{NO}_3\text{-N}$). The basic idea of an ecosystem model is to define the biomass of all organisms in terms of the mass of carbon per unit volume and to formulate the matter cycle based on the biochemical interactions shown in Figure 2 by using mass balance equations. When biochemical processes are represented by first-order kinetics, the resulting equations are given as a first-order ordinary equation for the concentration variation per unit time. As the water depth in the reservoir changes with time, the mass balance equations are not considered for the mass per unit volume but the whole quantity of reservoir capacity. When the reservoir's volume V is represented by the product of representative water surface area (= 2,560 m²) and the water depth h continuously measured at the center, the mass balance equations of phytoplankton, DIN, and DIP as examples, the main state variables were given as follows.

The carbon content of phytoplankton is gained by photosynthesis (growth) and lost by respiration, grazing by zooplankton, excretion, non-predatory mortality, and settling. As there is no inflow loading of algae from the

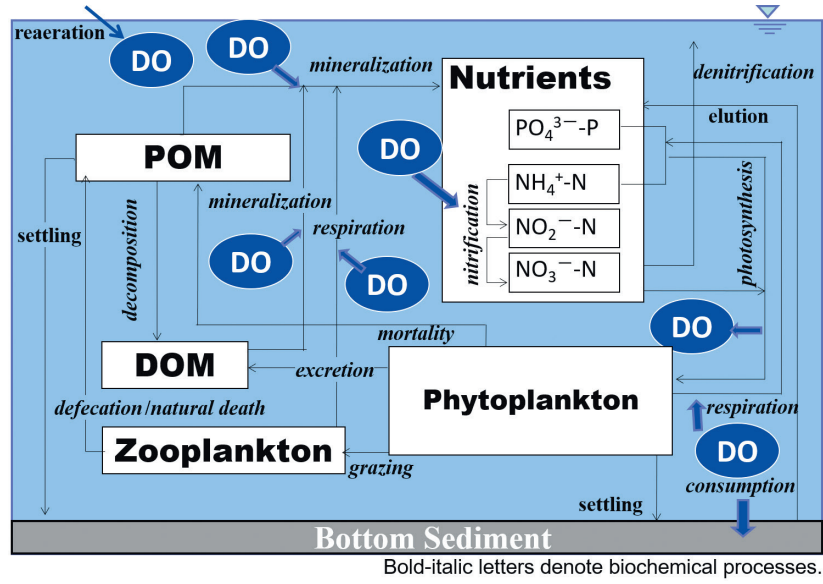


Fig. 2. Schematic layout of the one-box ecosystem model

upland farm, the mass balance for phytoplankton concentration C_{PP} is expressed as follows without considering the inflow loading of algae,

$$\begin{aligned} \frac{d(V C_{PP})}{dt} = & v_g V C_{PP} - v_{rp} V C_{PP} - v_{gz} V C_{ZP} - v_e V C_{PP} \\ & - v_{npm} V C_{PP} - \frac{w_{PP}}{h} V C_{PP} \end{aligned} \quad (1),$$

where v_g is the photosynthesis rate, v_{rp} is the respiration rate, v_{gz} is the grazing rate for zooplankton, v_e is the excretion rate, v_{npm} is the rate of non-predatory mortality, and w_{pp} is the settling velocity.

DIP and DIN are gained due to respiration from phytoplankton and zooplankton and mineralization of POM and DOM; they are lost by photosynthesis in phytoplankton. Furthermore, considering the elution of $\text{NH}_4\text{-N}$ and $\text{PO}_4\text{-P}$ from the bottom sediment as well as inflow and outflow loadings, and the mass balances for nutrient concentrations C_{DIPorDIN} can be written as follows:

$$\begin{aligned} \frac{d(V C_{\text{DIPorDIN}})}{dt} = & [\text{PorN: } C_{PP}] v_{rp} V C_{PP} \\ & - [\text{PorN: } C_{PP}] v_g V C_{PP} + [\text{PorN: } C_{ZP}] v_{rz} V C_{ZP} \\ & + [\text{PorN: } C_{\text{POM}}] v_{mip} V C_{\text{POM}} \\ & + [\text{PorN: } C_{\text{DOM}}] v_{mid} V C_{\text{DOM}} + V \frac{F_{\text{DIPorDIN}}}{h} \\ & + L_{\text{in,DIPorDIN}} - L_{\text{out,DIPorDIN}} \end{aligned} \quad (2),$$

where $[\text{P or N:C}_{PP}]$, $[\text{P or N:C}_{ZP}]$, $[\text{P or N:C}_{\text{POM}}]$, and $[\text{P or N:C}_{\text{DOM}}]$ are the respective mass ratios of phosphorus-to-carbon or nitrogen-to-carbon in chlorophyll-a, zooplankton, POM, and DOM; v_{rz} is the respiration rate of zooplankton, v_{mip} and v_{mid} are the respective mineralization rates of POM and DOM, F_{DIP} and F_{DIN} are the elution flux of DIP and DIN from the bottom sediments, and $L_{\text{out,DIPorDIN}}$ is the inflow and outflow loadings of DIP and DIN. In this research, the inflow load of nutrients due to deposition from the atmosphere was ignored because the site experiences minimal atmospheric nutrient deposition due to low industrial activity and geographical features. This decision was also made to isolate the impact of agricultural runoff without interference from atmospheric deposition, thus accurately assessing its contribution to nutrient loading.

The first-order rate constants, represented by the symbol v , can be defined as functions of water temperature $v = \alpha \cdot \exp(\beta T)$, where T is the water temperature, α is a rate constant at 0°C , and β is a temperature coefficient, except for mineralization, elution, and photosynthesis. The mineralization rate and elution flux can be defined by the exponential curve in combination with an effect of the DO concentration. As photosynthesis is mainly affected by water temperature, underwater light intensity, and nutrient concentration of DIN and DIP, these three environmental factors can be considered in the definition of growth rates. That is, v_g is represented in the consideration with limiting factors on photosynthesis as $v_g = \alpha_g \cdot f_T \cdot f_I \cdot f_N$, where α_g is the maximum growth rate, f_T , f_I , and f_N denote the limitation

functions of water temperature, light, and nutrients, respectively. The limitation functions can be defined from 0 to 1, representing the positive influence against phytoplankton growth. For example, the smaller the value f_T , the greater the growth inhibition due to temperature. Generally, f_T is defined using an optimal temperature T_{opt} as follows (Nguyen et al. 2010, Bui & Dang 2020)

$$f_T = \left\{ \frac{T}{T_{opt}} \exp \left(1 - \frac{T}{T_{opt}} \right) \right\}^\xi \quad (3),$$

where ξ is a constant generally determined in the range of 1 to 3. The relationship between the photosynthetic rate and light intensity can be represented with Steel's equation (Steel 1965). When the vertical profile of underwater light intensity can be represented by the Lambert-Beer law, the light limitation function for the light intensity averaged for the whole depth can be expressed based on Steel's equation as follows:

$$f_I = \frac{1}{\kappa h} \left\{ \exp \left(1 - \frac{I_0}{I_{opt}} \exp(-\kappa h) \right) - \exp \left(1 - \frac{I_0}{I_{opt}} \right) \right\} \quad (4),$$

where I_{opt} is the optimal light intensity, I_0 is the solar radiation at the water surface, and κ is the extinction coefficient of underwater light intensity. The above equation shows that the photosynthetic rate reaches a maximum at the optimal light intensity and that phytoplankton growth has a strong light-inhibiting characteristic when $I > I_{opt}$. Furthermore, the growth limitation functions for DIN and DIP can be described by the Michaelis–Menten equation and Liebig's law of the minimum as follows:

$$f_N = \min \left(\frac{C_{DIP}}{K_{DIP} + C_{DIP}}, \frac{C_{DIN}}{K_{DIN} + C_{DIN}} \right) \quad (5),$$

where K_{DIN} and K_{DIP} are half-saturation constants. The above equation expresses that the least available nutrient determines growth.

The model parameters, for example, the biochemical reaction rate constant and the mass ratios such as [P:C_{pp}], were set in relation to previous studies (Nguyen et al. 2010, Bui & Dang 2020). They were calibrated by trial-and-error adjustment to best match trends in the observed water quality data in 2019 and 2021. A dominant single species in the general ecosystem model would be considered a typical phytoplankton through all seasons. It is difficult to consider algal species' diversity and the seasonal change of the dominant algae. However, it is hard to handle the typical phytoplankton in the long term

over several months in the eutrophic water areas where actual dominant species drastically vary in multiple algal classes (Chlorophyceae, Cyanobacteria, diatoms, etc). Particularly, the difficulty of model application to the hypertrophic water area would be more conspicuous because algal blooms abruptly appear or disappear in response to meteorological conditions in the heating season. Therefore, it is required to uniquely determine the parameters related to the photosynthesis for the seasonal change such that the dominant species would alter significantly at algal class-differentiated levels corresponding to water temperature and solar radiation. In this study, several temperature zones were set, and the values of α_g , ξ , T_{opt} , K_{DIN} , K_{DIP} and I_{opt} were determined in each zone. By first setting the maximum growth rate α_g in the water temperature zones, it was possible to suppose that typical phytoplankton is a dominant species determined to correspond to the water temperature. Also, it was possible to reflect the typical phytoplankton to determine the model parameters, T_{opt} , K_{DIN} , K_{DIP} , and I_{opt} characterize the limitation functions by temperature, light, and nutrients. By handling model parameters, it would be expected that the significant changes in phytoplankton concentration corresponding to meteorological environment factors could be reproduced.

The Runge-Kutta-Gill method was applied to the numerical solution of the ordinary differential equations at 10-minute intervals to reproduce the periodically observed results of Chl-a. The initial condition of the model was set on July 2, 2019, and September 10, 2021, and the calculation period was 151 days and 104 days in 2019 and 2021, respectively. In the targeted reservoir, macroalgae, such as filamentous algae, flourished from spring to summer. However, it was proven to be challenging to incorporate macroalgae into the ecosystem model, so the initial condition was set after the disappearance of filamentous algae in both years. This simulation required observation data under the numerical conditions as follows. The time series data of water temperature, continuously measured at approximately 1.5 m below the water surface as an overall average value of the reservoir, was essential to consider the temperature dependency of biochemical rates. Also, the periodic observations of transparency D_s were applied to calculate an extinction coefficient of underwater light intensity by the relationship $\kappa = 1.7/D_s$. They were used to calculate the limitation functions expressed in Equation (4) together with the continuously observed results of solar radiation I_0 . Furthermore, the continuous measurements of water depth at the center were utilized not only for calculating the reservoir's volume V , but also for estimating the outflow discharge through broad crested

weirs by considering a difference of h from a weir height as an overflow depth to evaluate the outflow loadings of $L_{out,DIN}$, and $L_{out,DIP}$. In addition, the continuously measured inflow discharge via the box culvert was applied to the calculations of $L_{in,DIN}$ and $L_{in,DIP}$ using LQ equations.

This proposed water quality prediction model was applied to scenario analyses to assess how much the reduction of DIN and DIP inflow loadings influence the inhibition of phytoplankton overgrowth. The scenario was set up for the same period as the calculation period in the model. The seriousness of algal bloom occurring in autumn might be affected by the timings when the nutrient concentration in the reservoir's water would increase due to inflow loadings during heavy rainfall. In 2019, heavy rains in summer caused a significant influx of nutrients, leading to high levels of both DIN and DIP by September. In 2021, despite low summer rainfall maintaining low nutrient inflow, the concentration of both DIN and DIP increased from September due to substantial nutrient inflows from autumn rain. Based on the results of field observation in these two years, which will be discussed in more detail later, we set up two cases for scenario analysis. The case in 2019 was determined by focusing on the excessive inflow-loadings due to local severe rain in late summer. This scenario analysis was applied to assess the influence of controlling the high

DIN and DIP concentrations in late summer on the inhabitation of algal bloom in the case of little precipitation in autumn. The case in 2021 was set to evaluate how high concentrations of phytoplankton could be inhibited by reducing the excess inflow loadings of nutrients during the proliferation period of cyanobacteria in autumn. In each case, three scenarios were set up to quantitatively evaluate the responses of Chl-a concentration to changes in the inflow loading in 2019 and 2021 of 1) DIP only, 2) DIN ($\text{NH}_4\text{-N}$ and $\text{NO}_3\text{-N}$) only or 3) DIP and DIN together. The increase in the inflow loading of DIP and DIN in these scenarios was determined by multiplying the observed values with $(1 + \alpha/100)$, where α was the rate of change and was set from -100% to 50% at intervals of 10% .

Results and discussion

1. Seasonal characteristics of water quality parameters based on periodic field observations

Figure 3 shows periodically observed results of Chl-a concentrations and algal class-differentiated ratios of the average water surface points (north-side, center, and south-side) in 2019 and 2021. Additionally, the seasonal changes in the average of water quality observations (Chl-a, $\text{PO}_4\text{-P}$, $\text{NH}_4\text{-N}$, $\text{NO}_3\text{-N}$, and N/P ratio) at the water surface, the inflow discharge and

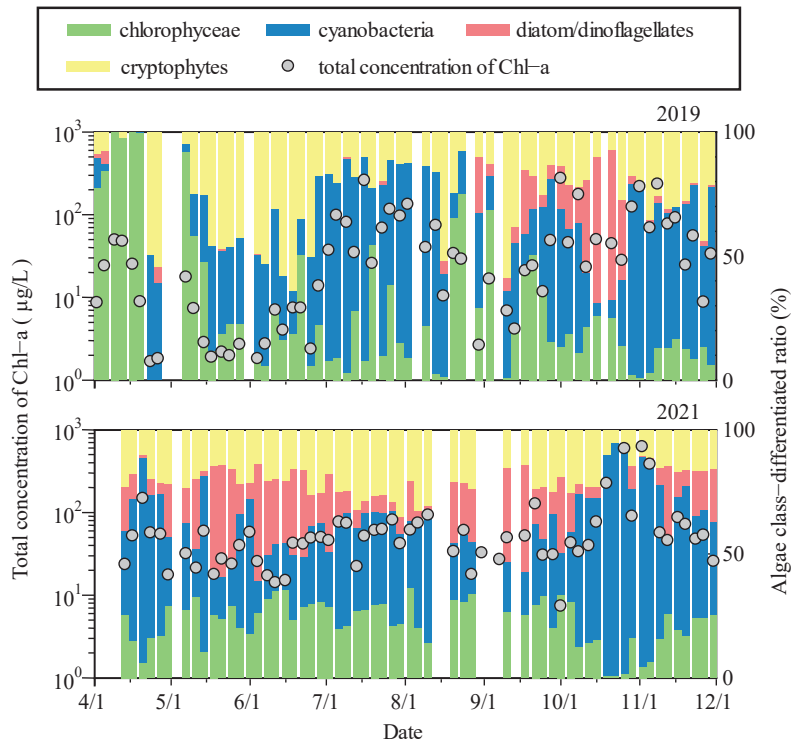


Fig. 3. Periodically measured Chl-a and algae class-differentiated ratio in 2019 and 2021 at the water surface

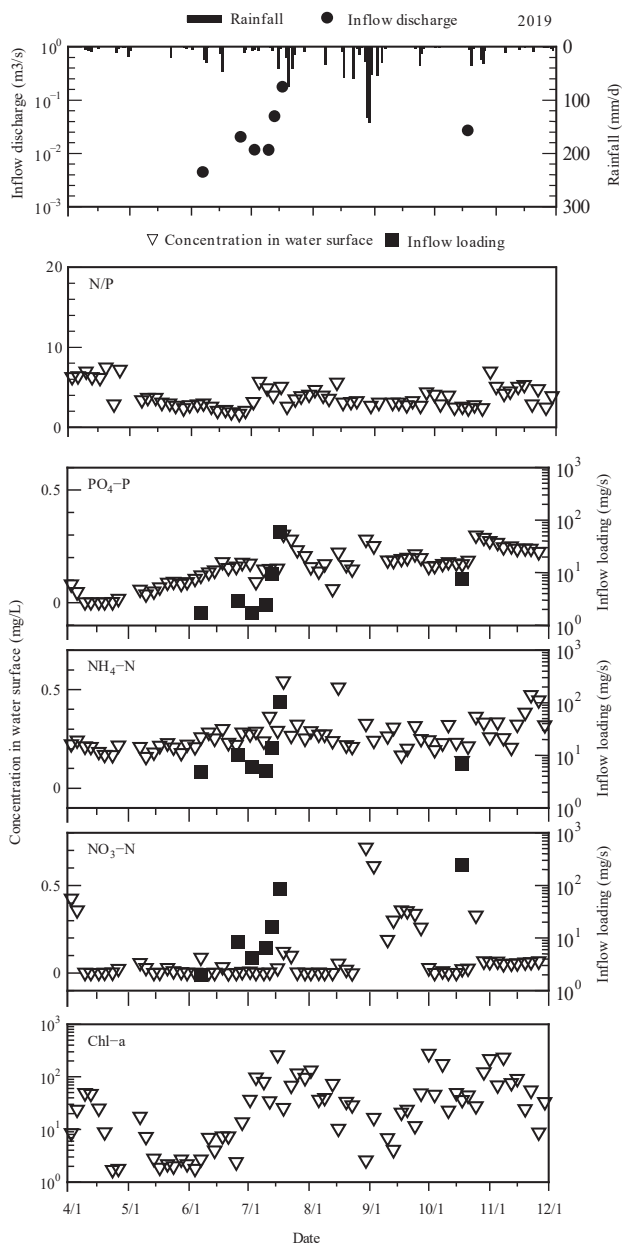


Fig. 4A. Rainfall, inflow discharge, and inflow loading observed results and Ratio of N/P, PO₄-P, NH₄-N, and NO₃-N, and Chl-a concentration at the water surface in 2019

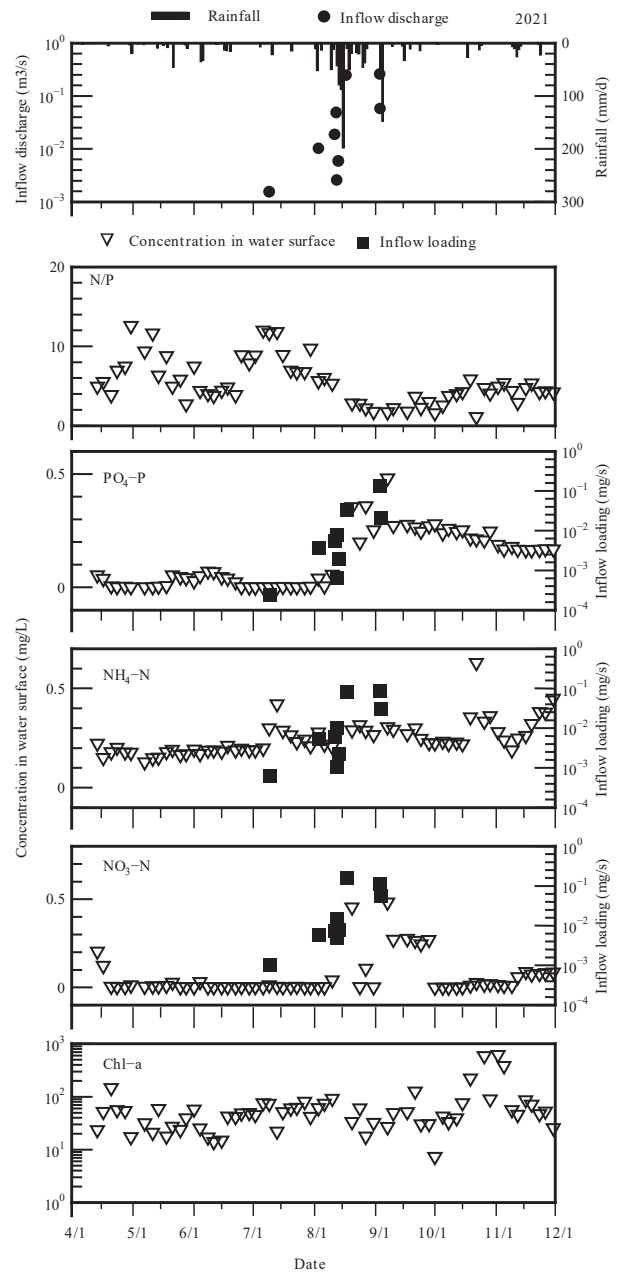


Fig. 4B. Rainfall, inflow discharge, and inflow loading observed results and Ratio of N/P, PO₄-P, NH₄-N, and NO₃-N, and Chl-a concentration at the water surface in 2021

inflow loadings of each type of nutrients, and the temporal changes in daily rainfall measured on the farmland near the targeted reservoir were summarized in Figure 4A for 2019 and Figure 4B for 2021. In Figure 4, the N/P ratio indicates the ratio of TN and TP. Furthermore, Figure 5 shows the water depth and transparency of the targeted reservoir in 2019 and 2021, and the LQ equations acquired based on the field observations are shown in Figure 6.

The descriptive statistical characteristics of the

above-observed results are summarized in Table 1. When comparing this table with the trophic status standard by OECD, the targeted reservoir was classified into the hypertrophic status (the average and maximum in Chl-a: more than 25 µg/L and more than 75 µg/L, the average in TP: more than 0.1 mg/L, and the average and minimum in transparency: less than 1.5 m and less than 0.7 m). However, applying the trophic classification to the OECD standard was not necessarily adequate without using full-year data. To supplement the judgment of the severity

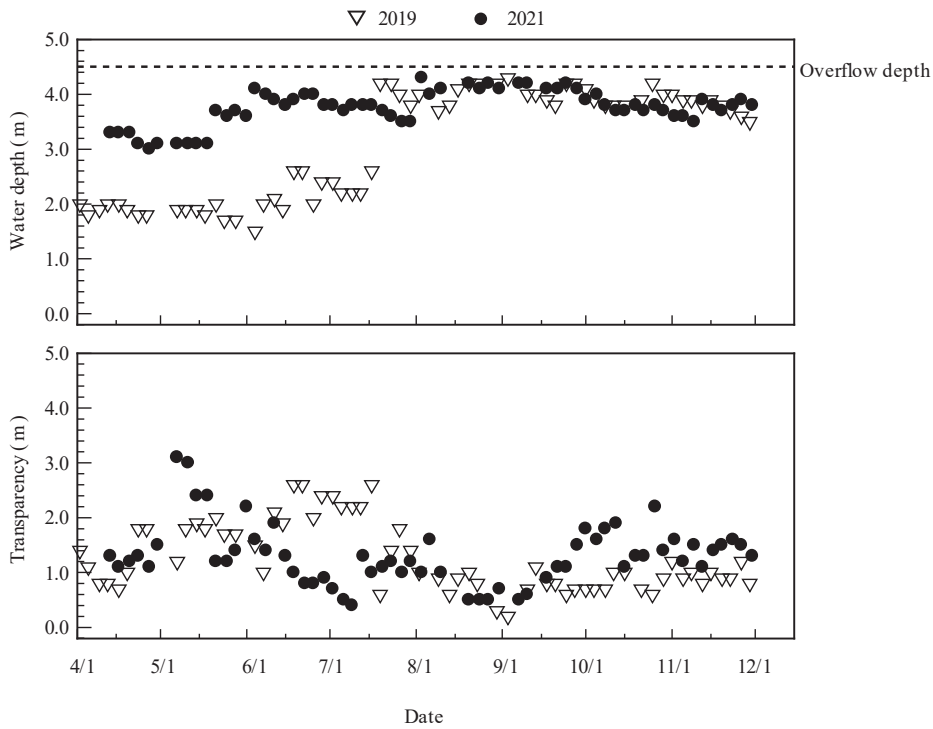


Fig. 5. Water depth and transparency of target reservoir in 2019 and 2021

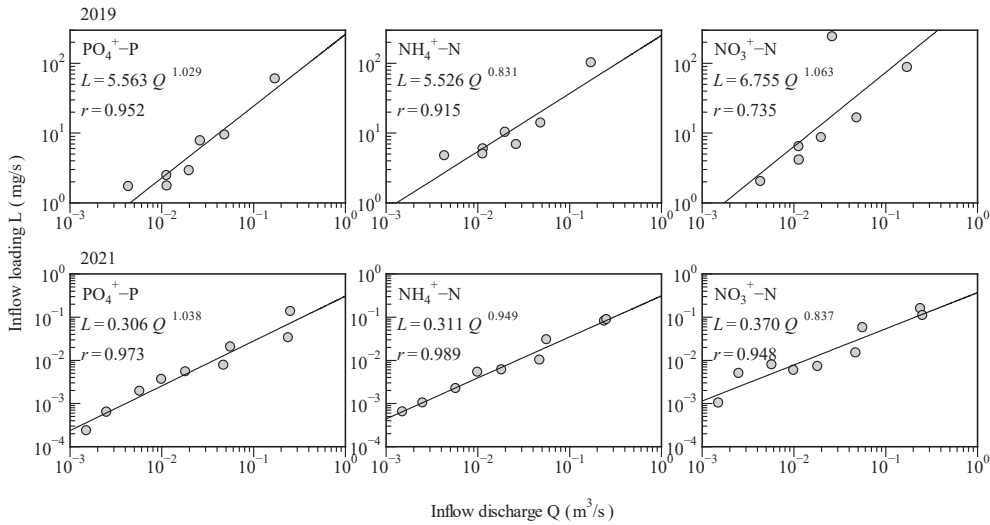


Fig. 6. Relational expression between inflow discharge Q and nutrient inflow load L (L-Q equation) in 2019 and 2021

of eutrophication, this study employed the trophic classification scheme by Forsberg & Ryding (1980). In this scheme, the trophic status could be classified by averages of TP, TN, Chl-a, and transparency in the summer season from June to September. As the observation period in this research was in a heating season and TN was included as a eutrophication index, the trophic classification scheme by Forsberg & Ryding (1980) seemed suitable for evaluating the water environment in the targeted reservoir. According to this

scheme, most of the water quality index in 2019 and 2021 exceeded the determination criteria of eutrophic status (TP: 0.25 to 0.1 mg/L, TN: 0.6 to 1.5 mg/L, Chl-a: 7 to 40 µg/L, and transparency: 1.0 to 2.5 m). Although the average TN in 2019 was 1.393 mg/L in the eutrophic range, its average value in the determinate period of June to September was 1.835 mg/L, or over the eutrophic range. Therefore, it was confirmed that the targeted reservoir was hypertrophic.

From Figure 3, the overall trend of seasonal changes

Table 1. The average, maximum, and minimum of main observed water environmental parameters in 2019 and 2021

Year		Chl-a ($\mu\text{g/L}$)	TP (mg/L)	$\text{PO}_4\text{-P}$ (mg/L)	TN (mg/L)	$\text{NO}_3\text{-N}$ (mg/L)	$\text{NH}_4\text{-N}$ (mg/L)	N/P
2019	Ave	48.9	0.345	0.158	1.393	0.089	0.267	3.776
	Max	696.9	2.253	0.309	10.709	0.829	0.557	15.433
	Min	1.3	0.030	0.005	0.363	0.000	0.044	1.265
2021	Ave	95.3	0.595	0.120	2.415	0.248	0.057	5.613
	Max	3847.0	21.923	0.486	44.560	1.183	0.486	15.424
	Min	4.9	0.028	0.002	0.296	0.113	0.001	0.900

**Fig. 7. Cyanobacteria blooms occurred on the water surface of the target reservoir in (A) October 2019 and (B) October 2021**

in Chl-a averaged on the water surface points (north-side, center, and south-side) bore a resemblance between 2019 and 2021 in that the concentration had significant fluctuation throughout the observation period in the wide order (2019: range of 10^0 to 10^3 and 2021: 10^1 to 10^3). The seasonal changes were characterized by three periods: the relatively low concentration period of April to June, in which a variation was significant due to large fluctuation, the increasing period of July to mid-November, and the decreasing period in late November. Chl-a increased in two steps from July to mid-November 2019 because of the temporal decrease from late August to early September. The remarkable point was that the Chl-a concentration in both years exponentially increased with a high temporal change rate. Its order ranged from 10^2 to 10^3 in summer and autumn, although it drastically lowered to 10^1 , together with the temporary decline of cyanobacteria from late August to early September. In the increasing period in 2019 and 2021, a dominance of cyanobacteria with an algae class-differentiated composition ratio of 60%-90% intermittently engendered the mat-like algal bloom over a wide range in two terms of July to early August and October to mid-November, as shown in Figure 7. In addition, both years had the characteristics in common in that the Chl-a averaged on water surface points exponentially increased to a peak value over the order of

10^2 in the autumn which included the maximum concentrations (2019: $696.9 \mu\text{g/L}$ and 2021: $3847.0 \mu\text{g/L}$) shown in Table 1, and that the increasing period was prolonged to mid-November even though the optimal water temperature for the cyanobacteria growth leans toward higher temperatures.

According to Figure 4A, the N/P ratio in 2019 changed from 2 to 7 (with an average of 3.8) throughout the observation period. According to Guildford & Hecky (2000), when the N/P ratio is less than 20, the nutrient status of the reservoir is determined as nitrogen limitation of growth. This denotes that the targeted water body was significantly nitrogen-limited in the aquatic ecosystem, as the balance between nitrogen and phosphorus necessary for photosynthesis was not maintained. Particularly, high Chl-a concentrations were sustained from July to mid-November without alleviation of nitrogen limitation. Additionally, in Figure 4B, the N/P ratio in 2021 exhibited a nitrogen-limiting condition, similar to 2019, throughout spring to autumn. However, there were differences between both years: the N/P ratio in 2021 varied from 1 to 14, and the nitrogen limitation was temporarily alleviated in May and July, unlike in 2019. The alleviation of nitrogen limitation in 2021 is linked to a balance between nitrogen and phosphorus available for photosynthesis. Nevertheless, an increase in Chl-a due to this balance was unclear, and the alleviation

of nitrogen limitation did not always lead to the apparent proliferation of phytoplankton. In the following discussion, we examined the responsiveness of Chl-a to the seasonal changes in nitrogen and phosphorus according to rainfall events as meteorological conditions based on Figure 4.

In 2019, PO₄-P exceeded 0.1 mg/L except for April and changed at a higher concentration than the DIP level in general eutrophic freshwater areas. Based on Figure 4A, it was evident that PO₄-P noticeably increased in response to rainfall events with daily precipitation exceeding 50 mm/d from mid-May. Consequently, such a rainfall event led to a significant increase in PO₄-P concentration exceeding 0.2 mg/L from July. Notably, during heavy rainfall events associated with the stagnant rainy season in mid-July and the linear precipitation zone in late August, PO₄-P levels increased to as high as 0.3 mg/L due to substantial inflow loadings from the watershed. According to the 2019 agricultural records at the experimental farm upstream of the targeted reservoir, DIP was intermittently applied as a supplementary fertilizer at multiple frequencies from April to November. Therefore, this excessive phosphorus fertilization, surpassing the adsorption ability in soil, seemed to result in a high concentration of PO₄-P in the targeted reservoir. This occurred because of an extensive inflow loading from agricultural fields through a box culvert. Moreover, during the increasing period of Chl-a in the summer, the reservoir received an excessive inflow loading of phosphorus. It was impossible to confirm a significant decrease in PO₄-P caused by algal uptake for photosynthesis. That is, the temporal excessive inflow loading of phosphorus is linked to an excessive nitrogen-limited status. On the other hand, NH₄-N in 2019 changed in the range of 0.25 to 0.4 mg/L with a slight increase due to inflow loading in mid-July and mid-August. However, there was no significant seasonal variation in the observation of NH₄-N. This result showed that the overall impact of inflow loading on NH₄-N concentration was minimal, and the decrease in NH₄-N due to uptake by algae was relatively small.

Meanwhile, NO₃-N temporally changed at a low level in the order of 10⁻² throughout the observation period except for a temporary increase over 0.1 mg/L during rainfall events in mid-July, late August, and late October. These sudden increases in NO₃-N concentration triggered by rainfall events rapidly lowered to zero within a few days or weeks when Chl-a stayed over 20 to 30 µg/L, corresponding to the maximum concentration in the hypertrophic status. The decreases in NO₃-N resulted from phytoplankton uptake as a nitrogen source for algal growth. Based on species composition at the algal class,

cyanobacteria likely dominated this uptake (Fig. 3). This consideration seemed identical to the understanding that cyanobacteria would preferentially utilize NO₃-N in DIN as a nitrogen source necessary for photosynthesis. Of particular note is the drastic and temporary increase of NO₃-N exceeding 0.7 mg/L derived from a rainfall event of approximately 200 mm/d at the end of August. This event seemed to impact the growth of cyanobacteria under intensive nitrogen-limited conditions, resulting in the prolonged occurrence of algal bloom until mid-November. In July, ammonium sulfate was applied as an additional fertilizer at the experimental farm. This application led to the inflow loading of NO₃-N derived from the nitrification of NH₄-N supplied in soil, significantly alleviating the substantial nitrogen limitation for the growth of cyanobacteria.

In Figure 4B, there were very few rainfall events exceeding 20 mm/d until July 2021, and it was considered that the impact of inflow loading on PO₄-P was extremely minimal during this period. Although temporary increases in PO₄-P over 0.1 mg/L due to some rainfall events in the period of mid-May to early June resulted in a relatively strong nitrogen-limited state with an N/P ratio of about 5, its concentration in the reservoir changed at the low level with the order of 10⁻². So, the relatively high N/P ratio over 10 in this period did not result from increased nitrogen concentration through the inflow loading. Instead, it was because phosphorus remained low, unaffected by the inflow loading of nutrients associated with rainfall events. However, Chl-a from April to July 2021 seasonally changed over 20 µg/L, unlike in 2019, and frequently reached a high concentration of about 80 µg/L. Therefore, until July, photosynthesis wasn't inhibited due to low concentrations of DIN and DIP, and the impact of decreases in nutrient inflow loadings on the phytoplankton growth was minimal. That is, the potential accumulation of nitrogen and phosphorus until the last year was confirmed, unlike in 2019. In addition, both NO₃-N and PO₄-P in the waterbody took high concentrations of approximately 0.5 mg/L during the heavy rainfall, including two events with precipitation of 150 to 200 mm/d in August and September. These results indicate the influence of heavy rainfall events on excess nutrient inflow loadings from fertilization in upstream agricultural fields. NO₃-N decreased sharply in late September and was kept at zero during the increasing period of Chl-a exceeding 100 µg/L from October.

In contrast, NH₄-N remained almost constant from September. These results suggest that the supply of NO₃-N via external loading promoted the growth of cyanobacteria, which would not require NH₄-N but

NO₃-N as a nitrogen source. PO₄-P in autumn was kept at a high concentration of around 0.2 mg/L, resulting in a substantial nitrogen limitation. However, it decreased from the peak value of heavy rainfall events in August and September.

It could be concluded from a common point in both 2019 and 2021 that the response of the phytoplankton, mainly including cyanobacteria, had an exceptionally sensitive response to the temporary supply of NO₃-N via the inflow loadings derived from heavy rainfall events while maintaining high PO₄-P concentrations exceeding 0.1 mg/L. This response led to a significant increase in Chl-a concentrations, reaching levels beyond the order of 10³. Therefore, the control of NO₃-N elevation during the summer and autumn periods in nitrogen-limited

eutrophic water bodies could link to crucial countermeasures for inhibiting cyanobacterial blooms in nitrogen-limited eutrophic water bodies.

2. Scenario analyses for water quality improvement using the ecosystem model

Comparisons of the calculated and the observed results of main variables, including Chl-a, DIP, and DIN, the observed results of water temperature and rainfall events, and the limitation function at actual simulation are shown in Figure 8. Also, the values of the model parameters (α_g , ξ , T_{opt} , K_{DIN} , K_{DIP} and I_{opt}) concerning the photosynthesis rate are summarized in Table 2. As described above, the parameter is generally determined to be in the range of 1 to 3. ξ However, in the target

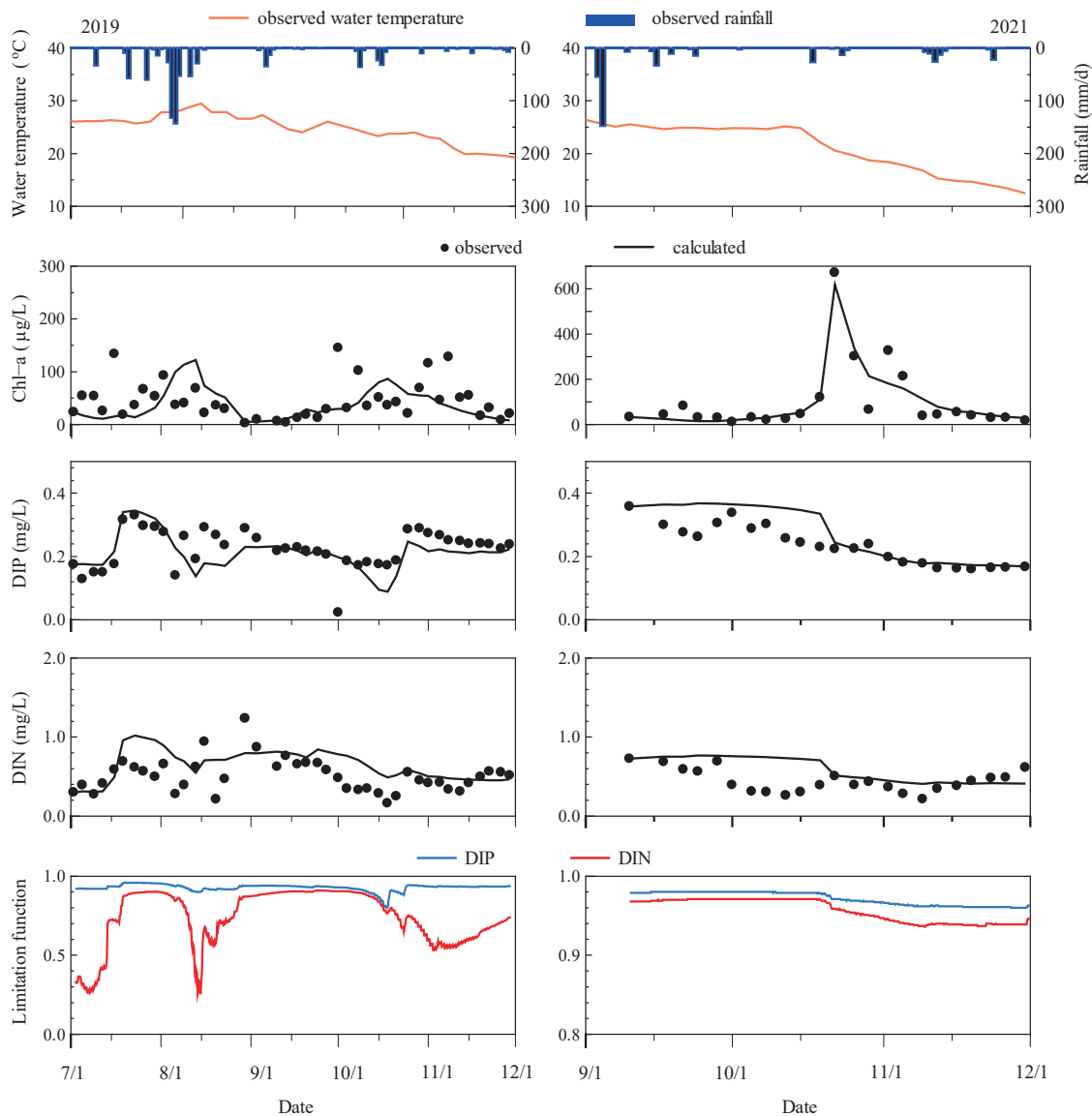


Fig. 8. Observed results of water temperature and rainfall, the comparison of calculated and observed changes of Chl-a, DIP, DIN, and the limitation function in actual simulation in 2019 and 2021

Table 2. Setting values of model parameters concerning the photosynthesis rate

Water temperature zones	ξ	T_{opt} (°C)	α_g (1/d)	I_{opt} (W/m ²)	K_{DIP} (mg/L)	K_{DIN} (mg/L)
$T \geq 25.0$	5.0	32.0	8.5	20.0		
$21.0 \leq T < 25.0$	4.0	30.0	8.0	20.0		
$19.0 \leq T < 21.0$	2.0	25.0	3.5	35.0	0.0075	0.012
$12.0 \leq T < 19.0$	3.0	25.0	3.0	35.0		
$T < 12.0$	2.0	21.0	2.0	35.0		

reservoir, the concentration of Chl-a was extremely high, exceeding 100 µg/L, a level typically not observed in general reservoirs. Therefore, it was necessary to set the value of ξ to be larger than the general range to reproduce this abnormal algae growth. The observation results in the figure are the values obtained by averaging the measurement results of the water at the surface and the bottom. The results indicate the model's robustness and precision in replicating observed trends in Chl-a concentrations over time. The model successfully mirrored the growth and decline patterns in Chl-a during seasonal changes, capturing notable events such as increases from July to August, a surge from early September to the end of October, and decreases from November onwards in 2019. Similarly, in 2021, the model accurately replicated the sudden Chl-a concentration fluctuations in late October, stable periods from mid-September to mid-October, and reductions during late November.

That is, it was possible to satisfactorily simulate the Chl-a dynamic by determining model parameters α_g , ξ , T_{opt} , and I_{opt} without adjusting values of K_{DIN} and K_{DIP} according to temporal changes in water temperature. Setting parameters of equation (3) in each water temperature zone led to reproduce, to some extent, sharp fluctuations in the concentration of Chl-a together with a large transformation in the existence ratio of cyanobacteria. However, such results were never reproduced by determining the model parameter as a constant throughout the calculation period. However, there was a need to examine whether the division of temperature zones and setting parameter values was appropriate from the viewpoint of algology. Moreover, the model effectively accounted for the influence of external factors such as heavy rainfall events, accurately predicting DIP and DIN concentration spikes in response to these occurrences in 2019 and 2021. While there were minor discrepancies in the simulation of DIP and DIN attributed to challenges in assuming perfectly mixed water due to changing weather conditions, the model's overall performance remained strong. In the actual phenomenon, the inflow loading of DIP and DIN came in

from the box culvert, spreading out over a small area. However, in the model, we considered the inflow loading to mix suddenly throughout the entire water body. That is why there was a period when the reproducibility of DIN/DIP was low due to the complete mixture model. The growth limitation function of nutrients is determined by lower values of the Michaelis–Menten equation of DIN and DIP, as shown in Equation (5). Figure 8 illustrates each growth limitation function value of DIN and DIP. In both 2019 and 2021, the limitation function of DIN consistently remained lower than DIP throughout the experimental period, indicating that the reservoir was experiencing nitrogen limitation, consistent with field observation findings. Therefore, the ecosystem model is deemed suitable to effectively predict the seasonal prevalence of phytoplankton and nutrients in this hypereutrophic reservoir. Based on the results of the inflow loadings, the study could be conducted successfully in different scenarios.

Figure 9 illustrates the simulated condition based on 2019 results, examining the rate of change in the average concentration of Chl-a when altering nutrient inflow loadings in three scenarios: DIP only (Fig. 9A), DIN only (Fig. 9B), and DIP and DIN together (Fig. 9C). In Figure 9A, a 30% reduction in DIP concentration has no immediate impact on the average Chl-a concentration, indicating stability. However, a discernible decrease in Chl-a concentration occurs when the DIP reduction is over 30%, signaling a shift from nitrogen to phosphorus limitation. The Chl-a concentration reaches the eutrophic level, as defined by OECD standards (Ave: 8-25 µg/L), with a 60% reduction in DIP loading. In the second scenario (Fig. 9B), when only DIN changes, there is a direct relationship between increasing DIN concentrations and a corresponding growth in Chl-a concentration, indicative of nitrogen limitation. Especially when DIN rises by 60% of the initial concentration, Chl-a reaches 60 µg/L, emphasizing the critical need to address nitrogen loading for effective algae control. Achieving a eutrophic Chl-a level (Ave: 8-25 µg/L) necessitates a significant 40% reduction in DIN loading. The third scenario, when changing both DIP and DIN, is shown in

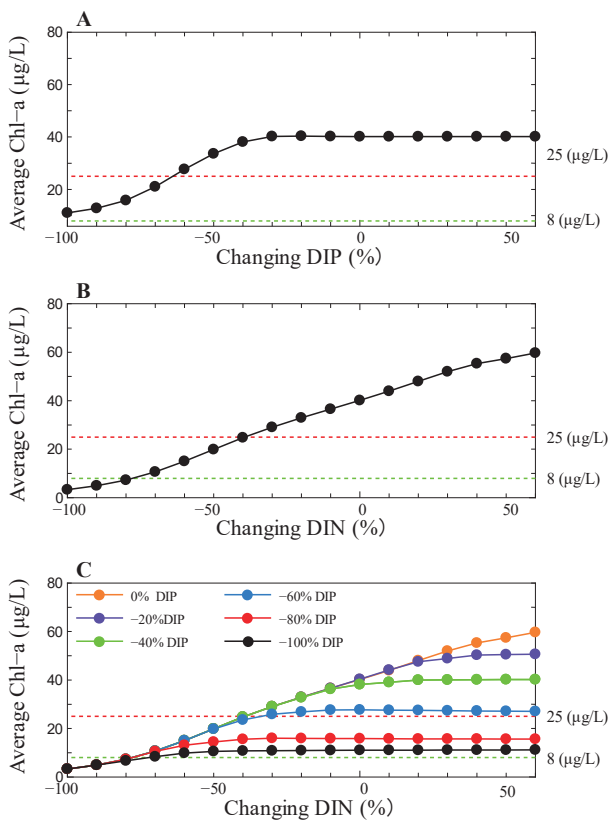


Fig. 9. Average Chl-a concentration changes with decreasing inflow loading of (A) DIP only, (B) DIN only, and (C) both DIP and DIN in 2019

Figure 9C. The effect of reducing the DIN load varies depending on the change rate in the DIP load. For example, when the DIP reduction rate is 40%, the decrease of DIN loading by 40% is necessary to reduce the average concentration of Chl-a to the eutrophic level. In addition, it is expected that Chl-a could reduce to a mesotrophic level (Ave: 2.5-8 µg/L) only by reducing 80% of the DIN load.

In the second condition in 2021, shown in Figure 10, the change rate in the Chl-a average concentration during the calculation period in each scenario was examined when the initial loadings of nutrients changed in three different scenarios: DIP only (Fig. 10A), DIN only (Fig. 10B), and DIP and DIN together (Fig. 10C). In Figure 10A, the Chl-a concentration remains steady with a 20% reduction in DIP from the initial concentration. However, a substantial decrease in Chl-a becomes noticeable when the DIP reduction exceeds 20%. If the DIP concentration drops by over 80% from the initial level, the reservoir's water quality could reach the eutrophic state (Ave Chl-a: 8-25 µg/L). Moving on to Figure 10B, the Chl-a concentration decreases to eutrophic levels when the DIN reduction surpasses 70% of the initial concentration. These findings underscore

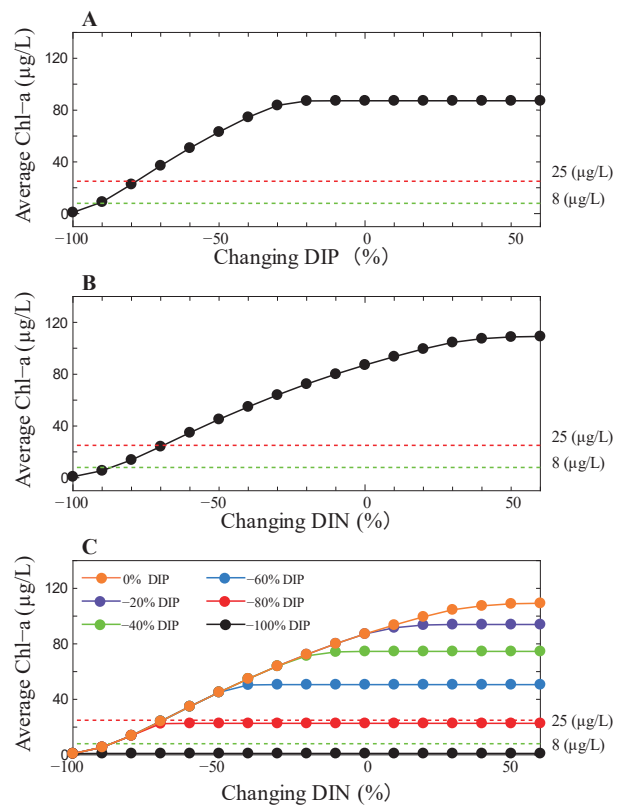


Fig. 10. Average Chl-a concentration changes with decreasing inflow loading of (A) DIP only, (B) DIN only, and (C) both DIP and DIN in 2021

the nitrogen-limited nature of the reservoir. In Figure 10C, when both the initial concentrations of DIP and DIN decrease simultaneously, maintaining Chl-a at the eutrophic level necessitates reductions of over 70% or 80% in DIP. Moreover, to bring Chl-a down to the mesotrophic level (Ave: 2.5-8 µg/L), it is imperative to reduce DIN concentrations by at least 90%.

Drawing insights from both scenarios, it becomes evident that in this reservoir with a limitation in nitrogen, diminishing nitrogen levels has a more pronounced effect in curbing phytoplankton growth than phosphorus reduction. The study's results highlight the importance of accurately identifying the limiting factor, whether nitrogen or phosphorus, within the reservoir's ecosystem. This understanding is key to implementing effective measures for preventing algal blooms.

Conclusion

This study provided novel evidence concerning the influence of nitrogen and phosphorous inflow loadings on the abnormal proliferation of phytoplankton through periodic observations and the actual status of aquatic environmental issues in the hypertrophic nitrogen-limited

reservoir. In particular, the seasonal change in phytoplankton, algae species dominance, nitrogen, and phosphorus levels were studied through water quality monitoring for two years in the reservoir where the long-term cyanobacteria blooms had occurred at the water surface during autumn. The water quality prediction model was constructed by considering the results obtained from the periodic water quality observations. This model provided scenario analyses to evaluate how to inhibit the occurrence of cyanobacterial blooms. The main outcomes obtained by this study can be summarized as follows:

From the observation results, the targeted reservoir was confirmed to be hypertrophic under nitrogen-limited conditions. Additionally, the temporal nitrogen loadings were the main cause of algal abnormalities. Severe hypereutrophication was confirmed with mat-like cyanobacteria blooms over a wide area in summer in 2019 and autumn in 2019 and 2021. Cyanobacteria was the dominant species throughout the two-year research period. The research observed a consistent trend in two years: phytoplankton, particularly cyanobacteria, displayed a remarkable sensitivity to temporary increases in nitrate-nitrogen (NO₃-N) caused by heavy rainfall. This sensitivity, combined with consistently high phosphate-phosphorus (PO₄-P) concentrations exceeding 0.1 mg/L, significantly elevated Chl-a levels, surpassing the order of 10³.

The validity of the ecosystem model was confirmed through two different cases. The first case was set based on the observation results in 2019 when the overgrowth of phytoplankton occurred mainly by the nutrient inflow loading due to rainfall in summer. The second was established using observation data in 2021 when nutrients from autumn rain events promoted abnormal phytoplankton growth. The Chl-a, DIP, and DIN simulation results successfully reproduced both the tendencies and seasonal changes of both cases. Therefore, the ecosystem model has high validity in effectively predicting the seasonal prevalence of phytoplankton growth in this hypereutrophic reservoir. The model successfully replicated certain sharp fluctuations in Chl-a levels, a phenomenon previously unattainable when employing a constant model parameter throughout the simulation period. However, further investigation is necessary to ascertain the suitability of segmenting temperature zones and assigning parameter values from an algological perspective. Thus, a future imperative lies in refining the categorization of water temperatures and aligning model parameters accordingly.

The trend of phytoplankton growth was predicted when the nutrient inflow loadings were changed in

different scenarios. The research outcomes demonstrate that in reservoirs characterized by nitrogen limitation, the reduction of nitrogen has a substantially more pronounced effect in curbing phytoplankton growth than reducing phosphorus levels. These findings emphasize the critical necessity of accurately identifying the limiting factor, whether nitrogen or phosphorus, within the reservoir's ecological system. This precise understanding is paramount in implementing targeted strategies to effectively prevent the occurrence of algal blooms.

References

- Aparicio Medrano, E. et al. (2016) An alternative explanation for cyanobacterial scum formation and persistence by oxygenic photosynthesis. *Harmful Algae*, **60**, 27-35.
- Bhagowati, B. & Ahamad, K. U. (2019) A review on lake eutrophication dynamics and recent developments in lake modeling. *Ecohydrol. Hydrobiol.*, **19**, 155-166.
- Bui, Q. L. & Dang T. T. (2020) Analysis of the principal factors affecting the algae growth in an urban eutrophic shallow lake by an ecosystem model. *Water Air Soil Pollut.*, **231**, 537.
- Correll, D. L. (1999) Phosphorus: a rate limiting nutrient in surface waters. *Poultry Sci.*, **78**, 674-682.
- Downing, J. A. & McCauley, E. (1992) The nitrogen: phosphorus relationship in lakes. *Limnol. Oceanogr.*, **37**, 936-945.
- Forsberg, C. & Ryding, S. (1980) Eutrophication parameters and trophic state indices in 30 Swedish waste-receiving lakes. *Arch. Hydrobiol.*, **80**, 189-207.
- García-Nieto, P. J. et al. (2019) Modeling algal atypical proliferation using the hybrid DE-MARS-based approach and M5 model tree in La Barca reservoir: A case study in northern Spain. *Ecol. Engin.*, **130**, 198-212.
- Guildford, S. J. & Hecky, R. E. (2000) Total nitrogen, total phosphorus, and nutrient limitation in lakes and oceans: Is there a common relationship? *Limnol. Oceanogr.*, **45**, 1213-1223.
- Hassanzadeh, E. et al. (2019) A framework for engaging stakeholders in water quality modeling and management: Application to the Qu'Appelle River Basin, Canada. *J. Environ. Manage.*, **231**, 1117-1126.
- Havens, K. E. & Walker, W. W. (2002) Development of a total phosphorus concentration goal in the TMDL process for Lake Okeechobee, Florida (USA). *Lake Reservoir Manage.*, **18**, 227-238.
- Jahan, R. et al. (2009) Study of harmful algal blooms in a eutrophic pond, Bangladesh. *Environ. Monitor. Assess.*, **170**, 7-21.
- Kotani, K. (1992) Chemistry and toxicity of microcystin. *Environ. Chem.*, **2**, 457-477 [In Japanese with English summary].
- Lamers, L. P. M. et al. (2013) Sulfide as a soil phytotoxin-a review. *Front. Plant Sci.*, **4**, 268.
- Nguyen, D. T. et al. (2010) Evaluation of the water-quality dynamics in a eutrophic agricultural pond using a one-box ecosystem model considering several algal groups. *Paddy Water Environ.*, **8**, 301-318.

- Organization for Economic Cooperation and Development (1982) Eutrophication of waters: Monitoring, assessment and control. Technical Report OECD. Environmental Directorate, OECD, Paris, DAS/DSI, **82**, 75-85.
- Ostrovsky, I. et al. (2020) Bloom-forming toxic cyanobacterium *Microcystis*: Quantification and monitoring with a high-frequency echosounder. *Water Res.*, **183**, 116091.
- Sharpley, A. N. et al. (2006) *Best management practices to minimize agricultural phosphorus impacts on water quality*. U.S. Department of Agriculture, Agricultural Research Service, ARS-163.
- Steel, J. H. (1965) Notes on some theoretical problems in production ecology. In Goldman C. R. ed., Primary production in aquatic environments, University of California Press, Berkeley, California, pp. 393-398.
- Zhang, P. et al. (2017) Hydrogen sulfide toxicity inhibits primary root growth through the ROS-NO pathway. *Sci. Rep.*, **7**, 868.